

Octahedral tilting induced frustration of c -axis order and proclivity towards ab -plane canted order in iridate heterostructures

Shubhajyoti Mohapatra,* Sreemayee Aditya, Rohit Mukherjee, and Avinash Singh

Department of Physics, Indian Institute of Technology, Kanpur - 208016, India

(Dated: June 25, 2019)

Iridate heterostructures are gaining interest as their magnetic properties are much more sensitive to structural distortion compared to pure spin systems due to spin-orbital entanglement induced by strong spin-orbit coupling. While bulk monolayer and bilayer iridates show ab -plane canted and c -axis antiferromagnetic (AFM) order, recent experiments on layered iridate superlattices (SL) have revealed striking properties, especially in the bilayer SL. A simplified spin model is presented for the bilayer SL including the tilting induced Kitaev type interactions, which illustrates the proclivity towards ab -plane canted AFM order. A realistic Hubbard model including all spin-dependent hopping terms arising from the octahedral rotation and tilting is constructed for the bilayer SL in the isospin space, and magnetic excitations are investigated in the self-consistently determined magnetic state. The Hubbard model analysis confirms the spin model results and shows strongly reduced magnon energy gap and an isospin reorientation transition from c -axis to ab -plane canted AFM order with increasing octahedral tilting.

PACS numbers: 75.30.Ds, 71.27.+a, 75.10.Lp, 71.10.Fd

I. INTRODUCTION

Strongly spin-orbit coupled systems are promising candidates for artificial heterostructures with leveraged magnetic properties arising from the sensitive coupling of magnetic moments to structural distortion.^{1,2} Recently, layered iridate superlattices $n\text{SIO}/1\text{STO}$ (with $n=1,2,3$) have been synthesized by stacking alternating layers of $n\text{SrIrO}_3$ and SrTiO_3 .³⁻⁷ Investigations on these heterostructures have provided insight into structural distortion effects on magnetic order, magnon energy gap, and magnetic order switching.

The monolayer and bilayer superlattices ($n\text{SIO}/1\text{STO}$, $n=1,2$) display canted antiferromagnetic (AFM) order (ab -plane for $n=1$, c -axis for $n=2$ with ferromagnetic moment in the ab plane). Although for $1\text{SIO}/\text{STO}$, this behaviour is similar to the bulk monolayer iridate, the significant ferromagnetic moment measured in $2\text{SIO}/1\text{STO}$ is attributed to the presence of octahedral tilting which induces canting of the c -axis AFM moments. Study of magnetic excitations by resonant inelastic x-ray scattering (RIXS)⁷ shows that both superlattices have similar magnon dispersions within experimental resolution. Both samples show finite magnon gap at (π, π) . While the magnon gap (≈ 32 meV) for $1\text{SIO}/1\text{STO}$ is nearly same as for Sr_2IrO_4 , the measured gap (≈ 57 meV) for $2\text{SIO}/1\text{STO}$ is significantly reduced compared to the gap (≈ 90 meV)⁸ for the bilayer bulk compound $\text{Sr}_3\text{Ir}_2\text{O}_7$. This large reduction in magnon energy gap indicates emergence of new magnetic interactions due to structural distortions.

The octahedral tilting was identified as the important structural feature which distinguishes the bilayer superlattice from the bulk compound. While both bulk monolayer and bilayer iridates feature large in-plane octahedral rotations, there is no octahedral tilting in Sr_2IrO_4 and very small tilting in $\text{Sr}_3\text{Ir}_2\text{O}_7$.⁹ However, $2\text{SIO}/1\text{STO}$ shows large octahedral tilting, although this effect is negligible in $1\text{SIO}/1\text{STO}$.^{3,7,10} Recent pressure studies on the bulk bilayer iridate also show presence of octahedral tilting and magnon softening, supporting the key role of structural distortion.¹¹ Significant octahedral tilting was suggested in the above studies to be responsible for driving the bilayer bulk and superlattice (SL) systems from c -axis towards ab -plane AFM ordering.

Detailed theoretical investigations explicitly including the additional anisotropic interaction terms generated by the octahedral tilting in the SL have not been carried out. Earlier studies based on simplified spin models have considered the same type of anisotropic in-

teraction terms as for the bulk bilayer iridate, and have extracted changes in the SL by fitting with the magnon dispersion.⁷ In this work, we will therefore investigate the octahedral tilting induced proclivity towards the ab -plane canted AFM order as well as the magnon gap reduction using a realistic bilayer Hubbard model including appropriate spin-dependent hopping terms corresponding to octahedral rotation and tilting in the bilayer SL. The spin-dependent hopping terms incorporate the additional orbital mixings between the xy and the xz, yz orbitals induced by octahedral tilting.

The structure of the paper is as below. After briefly reviewing the microscopic origin of the additional anisotropic interaction terms for the bilayer SL in Sec. II, a simplified spin model is presented in Sec. III which reveals a reorientation transition from c -axis to ab -plane AFM order with increasing octahedral tilting. A realistic bilayer Hubbard model including appropriate spin-dependent hopping terms corresponding to octahedral rotation and tilting in the bilayer SL is introduced in Sec. IV. Electronic band structure, self-consistent determination of magnetic order, and magnon excitations are discussed in Secs. IV and V. Finally, some key conclusions are presented in Sec. VI.

II. OCTAHEDRAL TILTING AND ANISOTROPIC INTERACTIONS

While c -axis AFM order is stabilized in the bulk bilayer iridate, the 2SIO/1STO heterostructure is on the verge of a reorientation transition to ab -plane canted AFM order. This reorientation transition is driven by the octahedral tilting, and the microscopic origin of the relevant anisotropic spin interactions is briefly discussed below.

Due to strong SOC, the t_{2g} manifold is split into the effective $J = 1/2$ and $3/2$ sectors, of which only the half-filled $J = 1/2$ sector is magnetically active. The two isospin states for the $J = 1/2$ sector are given by:

$$\begin{aligned} |\tau = \uparrow\rangle &= (1/\sqrt{3})[|yz, \downarrow\rangle + i|xz, \downarrow\rangle + |xy, \uparrow\rangle] \\ |\tau = \downarrow\rangle &= (1/\sqrt{3})[|yz, \uparrow\rangle - i|xz, \uparrow\rangle - |xy, \downarrow\rangle] \end{aligned} \quad (1)$$

in terms of the local orbital-spin states $|\mu, \sigma\rangle$, where $\mu = yz, xz, xy$ and $\sigma = \uparrow, \downarrow$. The interplay of these SOC-induced spin-orbital-entangled states and the orbital mixing hopping terms generated by octahedral rotation and tilting is essentially responsible for the anisotropic magnetic interactions.

We first consider the staggered octahedral rotation (small angle α) about the c axis, which generates orbital mixing hopping terms $t_{ij}^{yz|xz} = -t_{ij}^{xz|yz}$ between neighboring sites i and j , where $t_{ij}^{yz|xz} \approx t_\pi \sin \alpha \cos \alpha \approx t_\pi \sin \alpha$, corresponding to π overlap between yz and xz orbitals. Using the above transformation, the hopping Hamiltonian:

$$T = - \sum_{\langle ij \rangle, \tau\tau'} |i\tau\rangle [t\mathbf{1} + i\sigma_z t_z]_{\tau\tau'} \langle j\tau' |, \quad (2)$$

where the usual spin-independent hopping term:

$$t = \frac{1}{3} \left(t_{ij}^{xz|xz} + t_{ij}^{yz|yz} + t_{ij}^{xy|xy} \right) = \frac{1}{3} (2t_\pi + t_\delta) \quad (3)$$

involving the π and δ overlaps of the yz, xz, xy orbitals, and the spin-dependent hopping term (with the Pauli matrix σ_z) arises from the orbital mixing hopping terms:

$$t_z = \frac{1}{3} \left(t_{ij}^{yz|xz} - t_{ij}^{xz|yz} \right) \approx \frac{2}{3} t_\pi \sin \alpha. \quad (4)$$

Including the local interaction term $Un_{i,\uparrow}n_{i,\downarrow}$, and carrying out the usual strong-coupling expansion for the half-filled Hubbard model up to second order in the hopping terms, yields the Kitaev-type $K_z(S_i^z S_j^z - S_i^x S_j^x - S_i^y S_j^y)$ and Dzyaloshinski-Moriya $2\sqrt{JK_z}\hat{z}\cdot(\mathbf{S}_i \times \mathbf{S}_j)$ interactions besides the usual isotropic Heisenberg interaction $J\mathbf{S}_i\cdot\mathbf{S}_j$, where $J = 4t^2/U$ and $K_z = 4t_z^2/U$.¹²

Similarly, octahedral tilting about the a and b crystal axes will generate orbital mixing hopping terms between the xy and the xz/yz orbitals, leading to spin-dependent hopping terms t_x and t_y , respectively. The hopping Hamiltonian in Eq. (2) will then include $i\sigma_x t_x$ and $i\sigma_y t_y$ contributions. Besides additional Kitaev-type and DM interactions, the t_x and t_y terms will generate symmetric-off-diagonal (SOD) interaction terms $\Gamma_{\alpha\beta}(S_i^\alpha S_j^\beta + S_i^\beta S_j^\alpha)$, where $\Gamma_{\alpha\beta} = 8t_\alpha t_\beta/U$ and $\alpha, \beta = x, y, z$. In the next section, these anisotropic interaction terms will be shown to be responsible for a octahedral tilting driven isospin reorientation transition.

III. SIMPLIFIED SPIN MODEL

We present here a simplified spin model which illustrates the proclivity towards ab -plane canted AFM order and the reduced magnon energy gap in the 2SIO/STO superlattice compared to the bulk bilayer iridate which shows robust c -axis AFM order. The simplified model

incorporates the critical role of the tilting induced Kitaev type interactions in the effective $J = 1/2$ spin model. The simplified spin model reveals a reorientation transition from c -axis to ab -plane canted AFM order with increasing octahedral tilting.

In the bulk monolayer and bilayer compounds, the octahedral tilting is negligible, and the three-orbital model therefore features only the orbital mixing hopping terms between the xz and yz orbitals arising from the staggered octahedral rotations about the c axis. This orbital mixing generates a spin-dependent hopping term, which results in anisotropic magnetic interactions in the strong coupling expansion. While the spin-dependent hopping term can be gauged away for the monolayer case (hence no true magnetic anisotropy), c -axis ordering with a large magnon gap is obtained in the bilayer case due to a frustration effect involving different canting proclivities for in-plane and out-of-plane neighboring spins.¹³

In contrast, the 2SIO/STO superlattice structure is characterized by both octahedral rotation as well as tilting which are comparable in magnitude, resulting in additional orbital mixing hopping terms between the xy orbital and the xz, yz orbitals. This leads to additional anisotropic magnetic interactions in the effective $J = 1/2$ spin model corresponding to the spin-dependent hopping terms $t_{x,y,z}$. We consider a simplified model on a square lattice:

$$\begin{aligned}
H_{\text{eff}} = & \sum_{\langle ij \rangle} \left[JS_i \cdot S_j + (K_z + K_c - K_x - K_y) S_i^z S_j^z \right. \\
& + (K_x - K_y - K_z) S_i^x S_j^x + (K_y - K_z - K_x) S_i^y S_j^y \\
& \left. + 2\sqrt{JK_z} (S_i^x S_j^y - S_j^x S_i^y) \right] \quad (5)
\end{aligned}$$

where K_c incorporates the effective c -axis anisotropy arising from the frustration in the bilayer compound due to the different canting proclivities of in-plane and out-of-plane neighboring spins. The last term is the Dzyaloshinski-Moriya interaction which is responsible for the ab -plane canting. We first consider several limiting cases in order to connect to the bulk monolayer and bilayer iridate compounds.

(1) $K_x = K_y = K_c = 0$: this case corresponds to the bulk monolayer iridate. For c -axis AFM order with $S_i^z = S$ and $S_j^z = -S$ on the two sublattice sites, the classical energy:

$$E^c = \sum_{\langle ij \rangle} - (J + K_z) S^2. \quad (6)$$

On the other hand, for ab -plane canted AFM order, with $S_i^x = -S_j^x = -S \cos \phi$ and $S_i^y =$

$S_j^y = S \sin \phi$ corresponding to canting angle ϕ , we obtain:

$$E^{ab}(\phi) = \sum_{\langle ij \rangle} \left(-J \cos 2\phi + K_z \cos 2\phi - 2\sqrt{JK_z} \sin 2\phi \right) S^2, \quad (7)$$

minimizing which with respect to ϕ yields:

$$\tan 2\phi = \frac{2\sqrt{JK_z}}{J - K_z} = \frac{2\sqrt{K_z/J}}{1 - K_z/J} = \frac{2 \tan \phi}{1 - \tan^2 \phi}. \quad (8)$$

The optimal canting angle is given by $\tan \phi^* = \sqrt{\frac{K_z}{J}} = \frac{t_z}{t}$, and the minimum energy:

$$E^{ab}(\phi^*) = - \sum_{\langle ij \rangle} (J + K_z) S^2 \quad (9)$$

is identical to the energy for c -axis AFM order. This degeneracy reflects the absence of true magnetic anisotropy and is responsible for the nearly gapless magnon mode in the bulk monolayer iridate compound.

(2) $K_c > 0$, $K_x = K_y = 0$: this case corresponds to the bulk bilayer iridate. The extra energy gain for c -axis order in this case breaks the degeneracy, resulting in true magnetic anisotropy and the large magnon gap in the bulk bilayer iridate.

(3) $K_c > 0$, $K_x > 0$, $K_y = 0$: this case corresponds to the bilayer iridate superlattice. When K_x becomes finite (due to octahedral tilting), the extra energy gain for c -axis AFM order is reduced to $(K_c - K_x)$, while there is an extra energy gain for ab -plane canted AFM order. This suggests that with increasing K_x , there must be a reorientation transition from c -axis to ab -plane canted AFM order.

For c -axis AFM order (with $S_i = S$ and $S_j = -S$), we obtain from Eq. (5):

$$E^c = - \sum_{\langle ij \rangle} (J + K_z + K_c - K_x) S^2, \quad (10)$$

whereas for the ab -plane canted AFM order (with $S_i^x = -S_j^x = -S \cos \phi$ and $S_i^y = S_j^y = S \sin \phi$):

$$E^{ab}(\phi) = \sum_{\langle ij \rangle} \left((-J + K_z) \cos 2\phi - K_x - 2\sqrt{JK_z} \sin 2\phi \right) S^2. \quad (11)$$

Minimization yields the same condition $\tan \phi^* = \sqrt{\frac{K_z}{J}}$ for the optimal canting angle ϕ^* , and we obtain for the minimum energy:

$$E^{ab}(\phi^*) = - \sum_{\langle ij \rangle} (J + K_z + K_x) S^2. \quad (12)$$

For $K_x = 0$, we have $E^c < E^{ab}(\phi^*)$, confirming the true magnetic anisotropy as in case (2). However, with increasing K_x , the energy difference decreases, and the ab -plane canted AFM order becomes the ground state for $K_x > K_x^*$, where the critical value:

$$K_x^* = K_c/2 \quad (13)$$

for the reorientation transition is simply related to the frustration-induced c -axis anisotropy term K_c .

(4) $K_c > 0$, $K_x = K_y > 0$: this is a more realistic case for the bilayer iridate superlattice accounting for octahedral tiltings around both a and b crystal axes. A general analysis for arbitrary polar angle θ will be carried out here, with $S_i^x = -S_j^y = -S \sin \theta \sin \phi$, $S_i^y = -S_j^x = -S \sin \theta \cos \phi$, and $S_i^z = -S_j^z = S \cos \theta$ for the A and B sublattice sites. This order accounts for the expected planar AFM order along the rotated $\hat{a}' = (\hat{a} + \hat{b})/\sqrt{2}$ direction and canting along the normal $\hat{b}' = (-\hat{a} + \hat{b})/\sqrt{2}$ direction. We obtain for the classical energy:

$$E(\theta, \phi) = \sum_{\langle ij \rangle} \left[-(J + K_z + K_c - 2K_x) \cos^2 \theta - \left((J - K_z) \cos 2\phi' + 2\sqrt{JK_z} \sin 2\phi' \right) \sin^2 \theta \right] S^2, \quad (14)$$

where $2\phi = \pi/2 + 2\phi'$. With the optimal canting angle given by $\tan \phi'^* = \sqrt{K_z/J}$, we obtain:

$$E(\theta, \phi^*) = \sum_{\langle ij \rangle} \left[-(J + K_z) - (K_c - 2K_x) \cos^2 \theta \right] S^2, \quad (15)$$

which has energy minimum at $\theta^*=0$ (c -axis order) for $K_x < K_c/2$ and at $\theta^*=\pi/2$ (ab -plane order) for $K_x > K_c/2$. The spin model analysis presented here provides a minimal realization of the octahedral tilting driven reorientation transition at the critical value $K_x^* = K_y^* = K_c/2$. The realistic bilayer Hubbard model analysis presented in the next section shows that the bilayer iridate SL may be quite close to this transition point.

Effects of the other anisotropic interaction terms associated with the octahedral tilting on the magnetic order is qualitatively discussed below. The Kitaev interactions generated by t_x and t_y are fully included above. The DM interactions $D_{x,y}(\hat{x} + \hat{y}) \cdot (\mathbf{S}_i \times \mathbf{S}_j)$ generated by t_x and t_y will generally induce spin canting. The SOD terms $-\Gamma_{xz}(S_i^x S_j^z + S_i^z S_j^x)$ and $-\Gamma_{yz}(S_i^y S_j^z + S_i^z S_j^y)$ (generated by the products $t_x t_z$ and $t_y t_z$) will contribute to AFM order in the x and y directions. These effects will be quantitatively investigated below within a realistic bilayer Hubbard model for the superlattice including spin-dependent hopping terms associated with octahedral rotation and tilting.

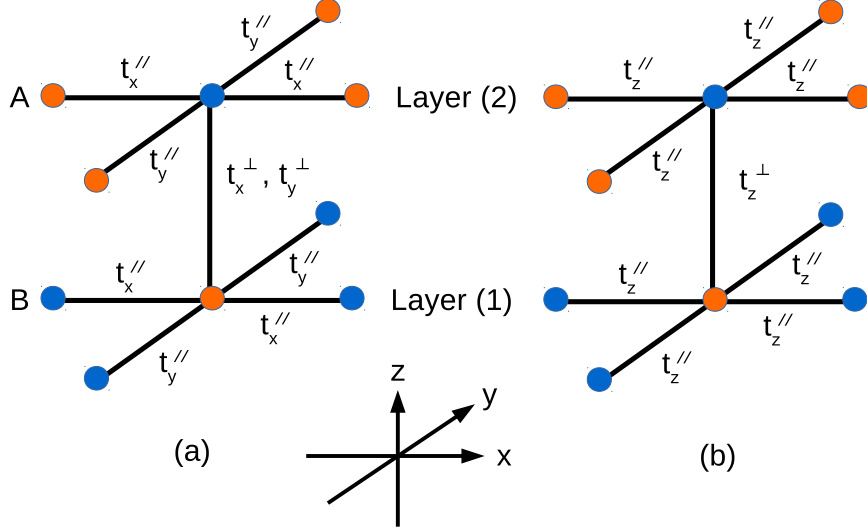


FIG. 1: The x, y components (a) and z component (b) of the spin-dependent hopping terms for intra- and inter-layer neighboring sites (indicated by \parallel and \perp). Here A and B denote the two magnetic sublattices. The spin-dependent hopping terms are antisymmetric ($\mathbf{t}'_{ji} = -\mathbf{t}'_{ij}$) due to the staggered octahedral rotation and tilting.

IV. BILAYER HUBBARD MODEL

For the 2SIO/1STO SL, we consider a minimal bilayer Hubbard model:

$$H = - \sum_{\langle ij \rangle, \sigma\sigma'} \left(t_{ij} \mathbf{1} + i \boldsymbol{\sigma} \cdot \mathbf{t}'_{ij} \right)_{\sigma\sigma'} a_{i\sigma}^\dagger a_{j\sigma'} + H.c. + U \sum_i n_{i\uparrow} n_{i\downarrow} \quad (16)$$

on a square lattice for each layer, where the sum $\langle ij \rangle$ includes intra-layer and inter-layer pairs of lattice sites i, j . Here t_{ij} and \mathbf{t}'_{ij} are the spin-independent and spin-dependent hopping terms, respectively. For t_{ij} , we have included first, second, and third neighbor intra-layer hopping terms ($t_1^\parallel, t_2^\parallel, t_3^\parallel$) and first neighbor inter-layer hopping term (t_1^\perp). Only the first neighbor spin-dependent hopping terms $\mathbf{t}'_{ij} = (t_x, t_y, t_z)$ are included, as shown in Fig. 1 for the intra- and inter-layer sites.

In the Hartree-Fock (HF) approximation, the interaction term reduces to a local exchange-field interaction:

$$\mathcal{H}_{\text{int}}^{\text{HF}} = \sum_{\mathbf{k}s} \psi_{\mathbf{k}s}^\dagger \left(-\boldsymbol{\sigma} \cdot \boldsymbol{\Delta}^s \right) \psi_{\mathbf{k}s} = \sum_{\mathbf{k}s} -\psi_{\mathbf{k}s}^\dagger \begin{pmatrix} \Delta_z^s & \Delta_x^s - i\Delta_y^s \\ \Delta_x^s + i\Delta_y^s & -\Delta_z^s \end{pmatrix} \psi_{\mathbf{k}s} \quad (17)$$

where $\psi_{\mathbf{k}s}^\dagger = (a_{\mathbf{k}s\uparrow}^\dagger, a_{\mathbf{k}s\downarrow}^\dagger)$, s is the composite layer-sublattice index corresponding to the two layers (1,2) and the two sublattices (A/B), and the exchange field components $\Delta_{x,y,z}^s$ are

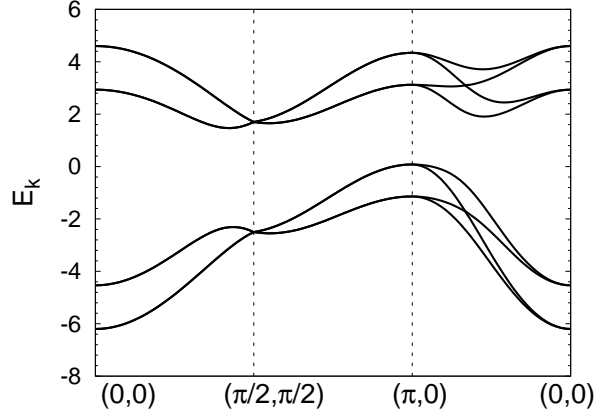


FIG. 2: Calculated electronic band structure in the self-consistent AFM state of the bilayer Hubbard model with hopping parameter values as given in Table I.

self-consistently determined from:

$$2\Delta_{x,y,z}^s = Um_{x,y,z}^s \quad (18)$$

in terms of the magnetization components.

We consider a composite 2-layer \otimes 2-sublattice \otimes 2-spin basis to represent the HF Hamiltonian matrix with appropriate hopping terms in the $\mathbf{k} = (k_x, k_y)$ space. For the self-consistent determination of the exchange field components, an iterative approach was employed starting with an initial choice for $(\Delta_x^s, \Delta_y^s, \Delta_z^s)$ with staggered order on the two layers and sublattices. In each iteration step, the local magnetization components were evaluated using the eigenvectors and eigenvalues of the Hamiltonian matrix, and the exchange field components were updated using Eq. (18).

The calculated electronic band structure in the self-consistent state is shown in Fig. 2 for the bilayer hopping parameter values given in Table I. The Coulomb interaction value $U = 5.2|t_1| \sim 0.8$ eV considered above is same as for the bulk bilayer compound.¹³ The calculated band structure is in qualitative agreement with DFT study for the 2SIO/1STO superlattice,⁴ including features such as valence band maximum at $(\pi, 0)$, conduction band minimum near $(\pi/2, \pi/2)$, overall bandwidth, and the band splitting structure.

The magnetization components obtained are: $(m_x^A, m_y^A, m_z^A) = (0.04, -0.119, 0.697)$ and $(m_x^B, m_y^B, m_z^B) = (0.119, -0.04, -0.697)$, indicating dominantly c -axis AFM order. Furthermore, finite ferromagnetic moment oriented along the a - b diagonal is evident from $(m_x^A + m_x^B) = -(m_y^A + m_y^B) \neq 0$ and $(m_z^A + m_z^B) = 0$. The bilayer magnetic order therefore

TABLE I: Bilayer hopping parameter values in terms of the energy scale unit $|t_1| = 150$ meV.

t_1^{\parallel}	t_2^{\parallel}	t_3^{\parallel}	t_x^{\parallel}	t_y^{\parallel}	t_z^{\parallel}	t_1^{\perp}	t_x^{\perp}	t_y^{\perp}	t_z^{\perp}
-1.0	0.3	-0.1	0.25	0.25	-0.2	-0.8	0.125	0.125	-0.6

corresponds to dominantly c -axis AFM order with ab -plane canting. This magnetic order will be referred to as phase I. The overall magnetic order in this phase is described by antiferromagnetic $\mathbf{m}_{\text{AF}} \equiv (\mathbf{m}_{\text{A}} - \mathbf{m}_{\text{B}})/2 = m_{\text{AF}}^c \hat{z} - m_{\text{AF}}^{\text{ab}}(\hat{x} + \hat{y})$ and ferromagnetic $\mathbf{m}_{\text{F}} \equiv (\mathbf{m}_{\text{A}} + \mathbf{m}_{\text{B}})/2 = m_{\text{F}}^{\text{ab}}(\hat{x} - \hat{y})$ components, which yields:

$$\begin{aligned} \mathbf{m}_{\text{A}} &= +m_{\text{AF}}^c \hat{z} - (m_{\text{AF}}^{\text{ab}} - m_{\text{F}}^{\text{ab}})\hat{x} - (m_{\text{AF}}^{\text{ab}} + m_{\text{F}}^{\text{ab}})\hat{y} \\ \mathbf{m}_{\text{B}} &= -m_{\text{AF}}^c \hat{z} + (m_{\text{AF}}^{\text{ab}} + m_{\text{F}}^{\text{ab}})\hat{x} + (m_{\text{AF}}^{\text{ab}} - m_{\text{F}}^{\text{ab}})\hat{y}. \end{aligned} \quad (19)$$

With increasing $t_{x,y}^{\parallel}$ and keeping $t_{x,y}^{\perp} = t_{x,y}^{\parallel}/2$, we find an isospin reorientation transition at a critical value (≈ 0.25) to a dominantly ab -plane canted AFM order which will be referred to as phase II. Near the critical value, self consistency required several thousand iterations. For $t_{x,y}^{\parallel} = 0.3$, the magnetization components obtained are: $(0.333, -0.594, -0.144)$ and $(-0.594, 0.333, -0.144)$ for the A and B sublattices, respectively. We have kept $t_{x,y}^{\perp} = t_{x,y}^{\parallel}/2$ to account for the nominally double orbital mixing hopping terms (π overlap) between xy and xz, yz orbitals for in-plane versus out-of-plane neighbors. The behavior of magnon excitations through the reorientation transition will be discussed in the next section.

V. MAGNON EXCITATIONS

In the following, we will investigate transverse spin fluctuations in the self-consistent magnetic state obtained above. We therefore consider the time-ordered magnon propagator:

$$\chi(\mathbf{q}, \omega) = \int dt \sum_i e^{i\omega(t-t')} e^{-i\mathbf{q}\cdot(\mathbf{r}_i - \mathbf{r}_j)} \langle \Psi_0 | T[S_i^{\mu}(t) S_j^{\nu}(t')] | \Psi_0 \rangle \quad (20)$$

involving the $\mu, \nu = x, y, z$ components of the isospin operators S_i^{μ} and S_j^{ν} at lattice sites i and j . In the random phase approximation (RPA), the magnon propagator is obtained as:

$$[\chi(\mathbf{q}, \omega)] = \frac{[\chi^0(\mathbf{q}, \omega)]}{1 - 2U[\chi^0(\mathbf{q}, \omega)]} \quad (21)$$

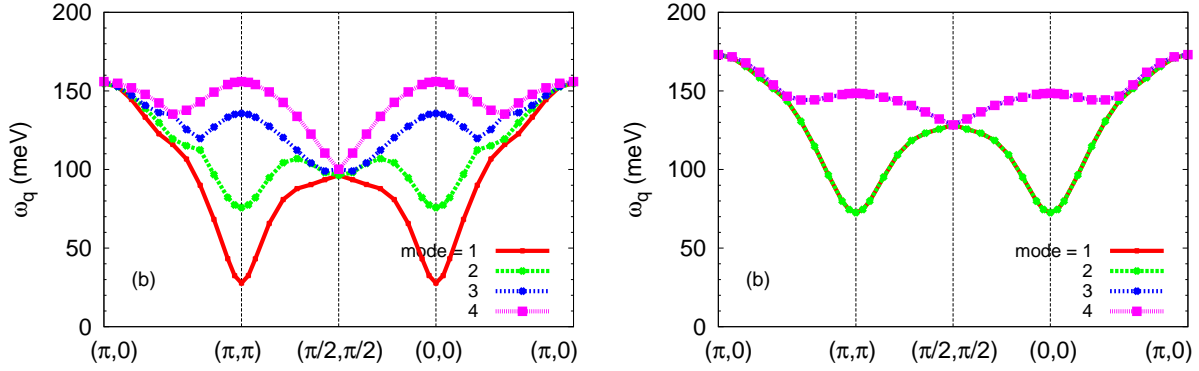


FIG. 3: Calculated magnon dispersions for the bilayer Hubbard model (a) with and (b) without the hopping terms t_x, t_y , showing strong magnon gap reduction (from 75 meV to 30 meV) induced by the octahedral tilting in the bilayer SL. Here, the reference case (b) corresponds to the bulk bilayer with reduced octahedral rotation effect but no tilting.

where the bare particle-hole propagator:

$$[\chi^0(\mathbf{q}, \omega)]_{ss'}^{\mu\nu} = \frac{1}{4} \sum_{\mathbf{k}} \left[\frac{\langle \varphi_{\mathbf{k}-\mathbf{q}} | \sigma^\mu | \varphi_{\mathbf{k}} \rangle_s \langle \varphi_{\mathbf{k}} | \sigma^\nu | \varphi_{\mathbf{k}-\mathbf{q}} \rangle_{s'}}{E_{\mathbf{k}-\mathbf{q}}^+ - E_{\mathbf{k}}^- + \omega - i\eta} + \frac{\langle \varphi_{\mathbf{k}-\mathbf{q}} | \sigma^\mu | \varphi_{\mathbf{k}} \rangle_s \langle \varphi_{\mathbf{k}} | \sigma^\nu | \varphi_{\mathbf{k}-\mathbf{q}} \rangle_{s'}}{E_{\mathbf{k}}^+ - E_{\mathbf{k}-\mathbf{q}}^- - \omega - i\eta} \right] \quad (22)$$

was evaluated in the composite spin-sublattice-layer basis (3 spin components \otimes 2 sublattices \otimes 2 layers) by integrating out the fermions in the self-consistent ground state. Here $E_{\mathbf{k}}$ and $\varphi_{\mathbf{k}}$ are the eigenvalues and eigenvectors of the Hamiltonian matrix, the indices $s, s' = 1, 4$ correspond to the layer-sublattice subspace, and the superscript $+(-)$ refers to particle (hole) energies above (below) the Fermi energy.

In the following, we will focus on the magnon energies $\omega_{\mathbf{q}}$ obtained from Eq. 21 using the magnon pole condition $1 - 2U\lambda_{\mathbf{q}}(\omega) = 0$, where $\lambda_{\mathbf{q}}(\omega)$ is the eigenvalue of the $[\chi^0(\mathbf{q}, \omega)]$ matrix. The 12×12 $[\chi^0(\mathbf{q}, \omega)]$ matrix was evaluated by performing the \mathbf{k} sum over the 2D Brillouin zone divided into a 300×300 mesh. Using this approach, magnon excitations were studied earlier for the bilayer bulk compound $\text{Sr}_3\text{Ir}_2\text{O}_7$.¹³ Two modes corresponding to acoustic and optical branches were obtained, with the acoustic mode showing a large magnon gap arising from the frustration effect due to different canting proclivities of in-plane and out-of-plane neighboring spins.

The calculated magnon dispersions for the bilayer Hubbard model is shown in Fig. 3, and compared for two cases corresponding to (a) the bilayer SL and (b) the bulk bilayer. For

the SL case, the magnon dispersion is calculated for the same hopping parameters (Table I) as for the band structure study. For the bulk case, the hopping terms $t_{x,y}^{\parallel}$ and $t_{x,y}^{\perp}$ were set to zero as the octahedral tilting is negligible. All other hopping terms were kept same for simplicity. For $t_z^{\perp} = -0.7$, we obtain magnon gap of ≈ 90 meV, as measured for the bilayer bulk compound $\text{Sr}_3\text{Ir}_2\text{O}_7$.⁸

Comparison of the calculated magnon dispersions therefore exclusively highlights the role of spin-dependent hopping terms t_x, t_y associated with octahedral tilting in the bilayer SL. The most important effect as seen in Fig. 3 is the strong magnon gap reduction from ~ 75 meV in the bulk bilayer case to ~ 30 meV in the bilayer SL. Correspondingly, the optical branch peak is pushed to higher energy. Also, the two-fold degeneracy in the bulk case is lifted, and the acoustic and optical modes are further split due to spin mixing.

Furthermore, all four branches in Fig. 3(a) are degenerate at $(\pi, 0)$ and $(\pi/2, \pi/2)$, where the energies are ~ 150 and 100 meV, respectively. The significant $(\pi, 0)$ magnon energy reduction from 170 meV in the bulk case to 150 meV in the SL case is due to minute enhancement in t_2^{\parallel} , which follows from the reduced octahedral rotation and therefore enhanced xy orbital overlap. These features are in excellent agreement with the RIXS spectra of 2SIO/1STO superlattice.⁷ Due to experimental limitations, the higher-energy magnon modes have not yet been experimentally resolved.

With increasing $t_x^{\parallel} = t_y^{\parallel}$ corresponding to the octahedral tilting, the magnon gap in the phase I decreases continuously to zero, as seen in Fig. 4(a). At the critical value (~ 0.25), there is reorientation transition from the dominantly c -axis AFM order to the dominantly ab -plane AFM order. The hysteresis behaviour near the transition point reflects the divergence in the number of iterations required for self consistency. The magnon gap in the phase II increases robustly from zero with $t_{x,y}^{\parallel}$ beyond the critical value. Thus, in addition to the self-consistent determination of the magnetic order, the magnon gap behaviour with $t_{x,y}^{\parallel}$ also correctly reflects the AFM I-II reorientation transition. In phase II, the magnon dispersion shows characteristic differences as seen in Fig. 4(b). Due to mixing between the acoustic and optical modes, the degeneracy is lifted near $(\pi, 0)$ and $(\pi/2, \pi/2)$ points.

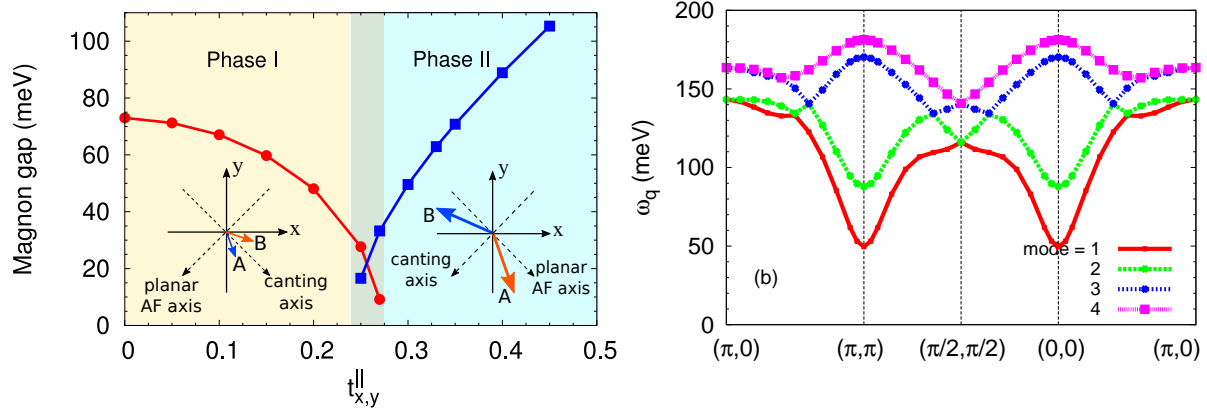


FIG. 4: (a) Strong magnon gap variation with the octahedral tilting induced hopping terms $t_{x,y}^{\parallel}$, showing the AFM I-II reorientation transition. (b) Magnon dispersion in the phase II for $t_{x,y}^{\parallel} = 0.3$. Inset in (a) shows only the planar part of the magnetic order. Phase I and II are dominantly c -axis and ab -plane AFM orders.

VI. CONCLUSIONS

A realistic bilayer Hubbard model was constructed to investigate magnon excitations in the bilayer iridate superlattice. The spin-dependent hopping terms arising from the octahedral tilting strongly suppress the magnon gap, driving the superlattice to the verge of a reorientation transition from c -axis to ab -plane canted AFM order.

A simplified spin model was presented which captures the essential features of the reorientation transition, and relates the critical value of the Kitaev type interaction term (K_x) induced by the octahedral tilting in the bilayer iridate superlattice to the effective c -axis anisotropy term (K_c) in the bilayer bulk compound. A critical value $K_x^* = K_c/2$ was found for the transition between the c -axis and ab -plane canted AFM orders. Our study indicates the possibility of magnetic order switching by tailoring the octahedral tilting in the bilayer iridate superlattice or via applied pressure for the case of bilayer bulk compound.

* Electronic address: shubhajm@iitk.ac.in

¹ H. Y. Hwang, Y. Iwasa, M. Kawasaki, B. Keimer, N. Nagaosa, and Y. Tokura, Nat. Mater. **11**, 103-113 (2012).

- ² J. Chakhalian, J. W. Freeland, A. J. Millis, C. Panagopoulos, and J. M. Rondinelli, *Rev. Mod. Phys.* **86**, 1189 (2014).
- ³ J. Matsuno, K. Ihara, S. Yamamura, H. Wadati, K. Ishii, V. V. Shankar, H.-Y. Kee, and H. Takagi, *Phys. Rev. Lett.* **114**, 247209 (2015).
- ⁴ S. Y. Kim, C. H. Kim, L. J. Sandilands, C. H. Sohn, J. Matsuno, H. Takagi, K. W. Kim, Y. S. Lee, S. J. Moon, and T. W. Noh, *Phys. Rev. B* **94**, 245113 (2016).
- ⁵ L. Hao, D. Meyers, C. Frederick, G. Fabbris, J. Yang, N. Traynor, L. Horak, D. Kriegner, Y. Choi, J.-W. Kim, D. Haskel, P. J. Ryan, M. P. M. Dean, and Jian Liu, *Phys. Rev. Lett.* **119**, 027204 (2017).
- ⁶ D. Meyers, K. Nakatsukasa, S. Mu, L. Hao, J. Yang, Y. Cao, G. Fabbris, H. Miao, J. Pelliciani, D. McNally, M. Dantz, E. Paris, E. Karapetrova, Y. Choi, D. Haskel, P. Shafer, E. Arenholz, T. Schmitt, T. Berlijn, S. Johnston, J. Liu, and M. P. M. Dean, *Phys. Rev. Lett.* **121**, 236802 (2018).
- ⁷ D. Meyers, Y. Cao, G. Fabbris, N. J. Robinson, L. Hao, C. Frederick, N. Traynor, J. Yang, J. Lin, M. H. Upton, D. Casa, J.-W. Kim, T. Gog, E. Karapetrova, Y. Choi, D. Haskel, P. J. Ryan, L. Horak, X. Liu, J. Liu, and M. P. M. Dean, *Sci. Rep.* **9**, 4263 (2019).
- ⁸ M. Moretti Sala, V. Schnell, S. Boseggia, L. Simonelli, A. Al-Zein, J. G. Vale, L. Paolasini, E. C. Hunter, R. S. Perry, D. Prabhakaran, A. T. Boothroyd, M. Krisch, G. Monaco, H. M. Rønnow, D. F. McMorrow, and F. Mila, *Phys. Rev. B* **92**, 024405 (2015).
- ⁹ T. Hogan, L. Bjaalie, L. Zhao, C. Belvin, X. Wang, C. G. Van de Walle, D. Hsieh, and S. D. Wilson, *Phys. Rev. B* **93**, 134110 (2016).
- ¹⁰ B. Kim, P. Liu, and C. Franchini, *Phys. Rev. B* **95**, 115111 (2017).
- ¹¹ J. Zhang, D. Yan, S. Yesudhas, H. Deng, H. Xiao, B. Chen, R. Sereika, X. Yin, C. Yi, Y. Shi, Z. Liu, E. M. Pärshcke, C.-C. Chen, J. Chang, Y. Ding, and H.-K. Mao, *npj Quantum Mater.* **4**, 23 (2019).
- ¹² S. Mohapatra and A. Singh, *J. Magn. Magn. Mater* **479**, 229 (2019).
- ¹³ S. Mohapatra, J. van den Brink, and A. Singh, *Phys. Rev. B* **95**, 094435 (2017).